Journal of Applied Physics

AIP Publishing

Parameter-free multiscale analysis of hydrogen solubility in Pd nano films under hydrogen gas using density functional theory

Akio Ishii[1, a)] and Nobutomo Nakamura[2]

[1)] *Graduate School of Engineering Science, Osaka University, 1-3 Machikaneyama, Toyonaka, Osaka 560-8531, Japan*

[2)] *Graduate School of Engineering, Osaka University, 2-1 Yamadaoka, Suita, Osaka 565-0871, Japan*

A parameter-free multiscale analysis of hydrogen solubility, hydrogen coverage, and hydrogen bulk concentration for face-centered-cubic Pd nano films with a (111) surface under hydrogen gas conditions is proposed using density functional theory and a simple kinetic model. The calculated solubility is quantitatively comparable to that obtained via experimental observations. Although the Pd surface is fully covered by hydrogen in a short time (microseconds to milliseconds) under exposure to 10–10000 ppm hydrogen gas pressure (1.0 atm), the hydrogen concentration in the subsurface or bulk changes significantly on the experimental time scale depending on gas pressure. We confirmed that the hydrogen concentration in the bulk or subsurface of Pd nano films (not the Pd surface) plays a role in the resistance change of Pd through comparison between the calculated hydrogen concentration and experimental observations of electric resistance change caused by exposure to hydrogen gas. A hydrogen sensor requires a 0.1 % change in the hydrogen concentration in the bulk to observe a significant change in the electric resistance. Further, we calculated the time-dependent diffusion coefficient of hydrogen in Pd nano film and compared it with experimental observed one. We also investigated temperature dependency of the solubility and confirmed that the hydrogen gas pressure determines hydrogen solubility in Pd nano films at the equilibrium state, whereas the temperature controls the speed to reach the equilibrium state.

[a)] Electronic mail: ishii@me.es.osaka-u.ac.jp

I. INTRODUCTION

Nanostructured materials (nanofilms or particles) have received significant attention from researchers because of their unique properties, and extensive experimental and theoretical studies have been conducted to develop nanomaterials with desirable characteristics[1–8]. Among such nanomaterials, Pd, Ag, and Au are typically used because of their stability, and Pd nanomaterials have emerged as promising candidates for hydrogen sensors and storage materials for the hydrogen society of the future because of their high ability to adsorb and absorb hydrogen[2,7,9–13]. Changes in the electrical resistance of Pd nanomaterials are conventionally used as a standard for sensing the existence of hydrogen[7,14–16]. Although significant resistance changes in Pd nanomaterials on exposure to hydrogen gas have been experimentally observed, the origin of resistance change and the role of hydrogen concentration in Pd nanomaterials remains unclear[14–17]. The nucleation of α–PdH_x ($x < 0.015$) inside the films is considered to be the reason for the resistance change in Pd nanofilms[7,14,17], in our recent study, we discussed the possibility that the increase in hydrogen coverage on the Pd surface is the origin of the resistance increase[16]. The effect of the subsurface of Pd on the resistance change has also been suggested previously[18,19]. We believe that this uncertainty is caused by the difficulty in investigating hydrogen solubility in Pd nanomaterials directly through experiments. Despite many theoretical studies on the ability of absorption and adsorption of the hydrogen[13,20,21], to the best of our knowledge, the direct and quantitative theoretical investigation of hydrogen solubility in Pd nano materials does not exist at present.

In this study, we propose a parameter-free multiscale analysis of hydrogen solubility in face-centered-cubic (FCC) Pd nanofilms with a (111) surface using the density functional theory (DFT) and kinetic model proposed by Davenport et al.[22]. All kinetic parameters, e.g., jump frequency and the activation energy of hydrogen diffusion in the kinetic model were energetically calculated using DFT atomistic simulations, achieving parameter-free (*ab initio*) analysis. The temporal evolution of hydrogen coverage on the surface and the concentration inside the Pd nano films under conventional temperature and hydrogen gas pressure conditions over a large time scale (from 10^{-15} to 10^{2} s) were investigated. The hydrogen coverage on the (111) surface and concentration at tetragonal (T sites) and octahedral sites (O sites) between each (111) layer were investigated in detail.

II. METHODOLOGY

A. Kinetic model

Fig. 1 shows the atomic structure of the FCC Pd nano film with (111) surface. We consider a Pd nano film with $N+1$ (111) atomic layers on a substrate, and the intermediate spacing between adjacent (111) layers is indexed as $1, 2, 3, \ldots, i, \ldots, N$ from the surface to the substrate. Once hydrogen molecules decompose into hydrogen atoms, the atoms are adsorbed on the (111) surface, and they prefer positions on top of the atoms in the second Pd (111) layer, as shown in the figure, referring to previous DFT studies[20,23]. Then, hydrogen atoms diffuse into the film through T sites in the subsurface and invade the inside of the Pd nanofilm through zigzag diffusion between the T and O sites in the intermediate spacing between the (111) layers as in the figure[21]. Based on this diffusion mechanism and the straightforward kinetic model proposed by Davenport et al.[22] and considering the net flux of hydrogen at each site, we constructed differential equations for the temporal evolution of the coverage and concentrations of hydrogen at each site between each (111) layer:

$$
\begin{aligned}
\frac{d\theta_{\mathrm{S}}}{dt} &= \{k_{(\mathrm{H_2}\to\mathrm{S})}(1-\theta_{\mathrm{S}})^2 - k_{(\mathrm{H_2}\leftarrow\mathrm{S})}\theta_{\mathrm{S}}^2\} - \{k_{(\mathrm{S}\to\mathrm{T}_1)}\theta_{\mathrm{S}}(1-\theta_{\mathrm{T}_1}) - k_{(\mathrm{S}\leftarrow\mathrm{T}_1)}\theta_{\mathrm{T}_1}(1-\theta_{\mathrm{S}})\},\\
\frac{d\theta_{\mathrm{T}_1}}{dt} &= \{k_{(\mathrm{S}\to\mathrm{T}_1)}\theta_{\mathrm{S}}(1-\theta_{\mathrm{T}_1}) - k_{(\mathrm{S}\leftarrow\mathrm{T}_1)}\theta_{\mathrm{T}_1}(1-\theta_{\mathrm{S}})\} - \{k_{(\mathrm{T}_1\to\mathrm{O}_1)}\theta_{\mathrm{T}_1}(1-\theta_{\mathrm{O}_1}) - k_{(\mathrm{T}_1\leftarrow\mathrm{O}_1)}\theta_{\mathrm{O}_1}(1-\theta_{\mathrm{T}_1})\},\\
\frac{d\theta_{\mathrm{O}_1}}{dt} &= \{k_{(\mathrm{T}_1\to\mathrm{O}_1)}\theta_{\mathrm{T}_1}(1-\theta_{\mathrm{O}_1}) - k_{(\mathrm{T}_1\leftarrow\mathrm{O}_1)}\theta_{\mathrm{O}_1}(1-\theta_{\mathrm{T}_1})\} - \{k_{(\mathrm{O}_1\to\mathrm{T}_2)}\theta_{\mathrm{O}_1}(1-\theta_{\mathrm{T}_2}) - k_{(\mathrm{O}_1\leftarrow\mathrm{T}_2)}\theta_{\mathrm{T}_2}(1-\theta_{\mathrm{O}_1})\},\\
&\vdots\\
\frac{d\theta_{\mathrm{T}_i}}{dt} &= \{k_{(\mathrm{O}_{i-1}\to\mathrm{T}_i)}\theta_{\mathrm{O}_{i-1}}(1-\theta_{\mathrm{T}_i}) - k_{(\mathrm{O}_{i-1}\leftarrow\mathrm{T}_i)}\theta_{\mathrm{T}_i}(1-\theta_{\mathrm{O}_{i-1}})\} - \{k_{(\mathrm{T}_i\to\mathrm{O}_i)}\theta_{\mathrm{T}_i}(1-\theta_{\mathrm{O}_i}) - k_{(\mathrm{T}_i\leftarrow\mathrm{O}_i)}\theta_{\mathrm{O}_i}(1-\theta_{\mathrm{T}_i})\},\\
\frac{d\theta_{\mathrm{O}_i}}{dt} &= \{k_{(\mathrm{T}_i\to\mathrm{O}_i)}\theta_{\mathrm{T}_i}(1-\theta_{\mathrm{O}_i}) - k_{(\mathrm{T}_i\leftarrow\mathrm{O}_i)}\theta_{\mathrm{O}_i}(1-\theta_{\mathrm{T}_i})\} - \{k_{(\mathrm{O}_i\to\mathrm{T}_{i+1})}\theta_{\mathrm{O}_i}(1-\theta_{\mathrm{T}_{i+1}}) - k_{(\mathrm{O}_i\leftarrow\mathrm{T}_{i+1})}\theta_{\mathrm{T}_{i+1}}(1-\theta_{\mathrm{O}_i})\},\\
&\vdots\ ,\\
\frac{d\theta_{\mathrm{O}_N}}{dt} &= k_{(\mathrm{T}_N\to\mathrm{O}_N)}\theta_{\mathrm{T}_N}(1-\theta_{\mathrm{O}_N}) - k_{(\mathrm{T}_N\leftarrow\mathrm{O}_N)}\theta_{\mathrm{O}_N}(1-\theta_{\mathrm{T}_N}).
\end{aligned}
\tag{1}
$$

Where θ_{S} (0–1) represents the hydrogen coverage on the (111) surface and θ_{T_i} and θ_{O_i} represent the hydrogen concentrations at the T and O sites in ith intermediate spacing, respectively ($i = 1, 2, 3, \ldots, N$). Each term on the right-hand side indicates the flux between two adjacent sites, including the Pd surface (indexed as "S") and the particle bath of the hydrogen molecule gas (indexed as " $\mathrm{H_2}$ "). Further, $k_{\mathrm{X}\to\mathrm{Y}}$ and $k_{\mathrm{X}\leftarrow\mathrm{Y}}$ in the equations

indicate the forward and backward transition rates from "X" to "Y" sites, respectively. $1-\theta_{\mathrm{X}}$ in the equations indicates how much space for hydrogen remained at the X site. Curly brackets indicate net flux changes between the two sites; e.g., $k_{(\mathrm{H_2}\rightarrow\mathrm{S})}(1-\theta_{\mathrm{S}})^2$ and $k_{(\mathrm{H_2}\leftarrow\mathrm{S})}\theta_{\mathrm{S}}^2$ in the first-line equation are in and out flux from the particle bath of the hydrogen molecule gas to the Pd (111) surface, and thus, $\{k_{(\mathrm{H_2}\rightarrow\mathrm{S})}(1-\theta_{\mathrm{S}})^2 - k_{(\mathrm{H_2}\leftarrow\mathrm{S})}\theta_{\mathrm{S}}^2\}$ indicates the net flux from the particle bath to the surface. These equations describe the temporal evolution of the hydrogen coverage on the (111) surface and hydrogen concentrations at the O and T sites in all intermediate spacings between the layers in Fig. 1. The temporal evolution at each site is described as the sum of its net flux between the adjacent sites, for example, the coverage is described as the sum of the net flux between the Pd (111) surface and particle bath and that between the Pd (111) surface and O sites in the subsurface, as in the first-line equation, because the Pd (111) surface contacts the particle bath and connects to T sites on the subsurface ($\mathrm{T_1}$), as shown in Fig. 1.

$k_{(\mathrm{H_2}\rightarrow\mathrm{S})}$ is the adsorption rate of hydrogen on the (111) surface and is described as[22]:

$$k_{(\mathrm{H_2}\rightarrow\mathrm{S})} = \frac{2\Gamma}{n_{\mathrm{S}}}\exp\left(-\frac{\Delta E_{(\mathrm{H_2}\rightarrow\mathrm{S})}}{k_{\mathrm{B}}T}\right). \tag{2}$$

where n_s, k_{B}, T, and $\Delta E_{(\mathrm{H_2}\rightarrow\mathrm{S})}$ represent the number of Pd atoms per unit area in each (111) layer, which can be determined crystallographically; Boltzmann's constant; temperature; and activation energy for hydrogen decomposition and adsorption on the (111) surface of the Pd nano film, respectively. We confirmed that both hydrogen decomposition and adsorption to the (111) surface of Pd nano films occur simultaneously using DFT atomistic simulations, and therefore, the transition can be described by a single activation energy value in this study. Γ indicates the flux of the molecules striking the Pd (111) surface, which can be described by the kinetic theory of gases[24,25].

$$\Gamma = \frac{p_{\mathrm{H_2}}}{\sqrt{2\pi m_{\mathrm{H_2}} k_{\mathrm{B}} T}}.$$

where $p_{\mathrm{H_2}}$ and $m_{\mathrm{H_2}}$ represent the partial pressure of the hydrogen gas and mass of the hydrogen molecule, respectively. For other $k_{\mathrm{X}\ \bigstar\ \mathrm{Y}}$ ($\bigstar$ is $\rightarrow$ or $\leftarrow$), we used the following Arrhenius form,

$$k_{(\mathrm{X}\ \bigstar\ \mathrm{Y})} = \nu_{(\mathrm{X}\ \bigstar\ \mathrm{Y})}\exp\left(-\frac{\Delta E_{(\mathrm{X}\ \bigstar\ \mathrm{Y})}}{k_{\mathrm{B}}T}\right). \tag{3}$$

where $\nu_{(\mathrm{X}\ \bigstar\ \mathrm{Y})}$ and $\Delta E_{(\mathrm{X}\ \bigstar\ \mathrm{Y})}$ represent the jump frequency and activation energy for the X to Y forward (or backward) transition, respectively. In this study, we calculated the

activation energies and jump frequencies of hydrogen diffusion (ΔE and ν) in the above differential equations using DFT atomistic simulation and temporal evolution of θ for the Pd (111) surface (coverage) and each site in each intermediate spacing between the (111) layers was numerically evaluated by setting the partial pressure of hydrogen p_{H_2} and temperature T as parameters. The calculation cost of the temporal evolution of θ using the above equations is very low, and a considerably long-term analysis of solubility change without any empirical parameters is possible. We implemented the analysis from 1.0×10^{-15} to 2.0×10^{2} s in this study. Note that we did not consider the surface diffusion of the hydrogen in our model because we confirmed that the activation energy of the surface diffusion is relatively low and negligible compared with that of the diffusion to subsurface using DFT atomistic simulation; the activation energy is lower than 0.1 eV and that of the diffusion to subsurface is 0.36 eV from Table I.

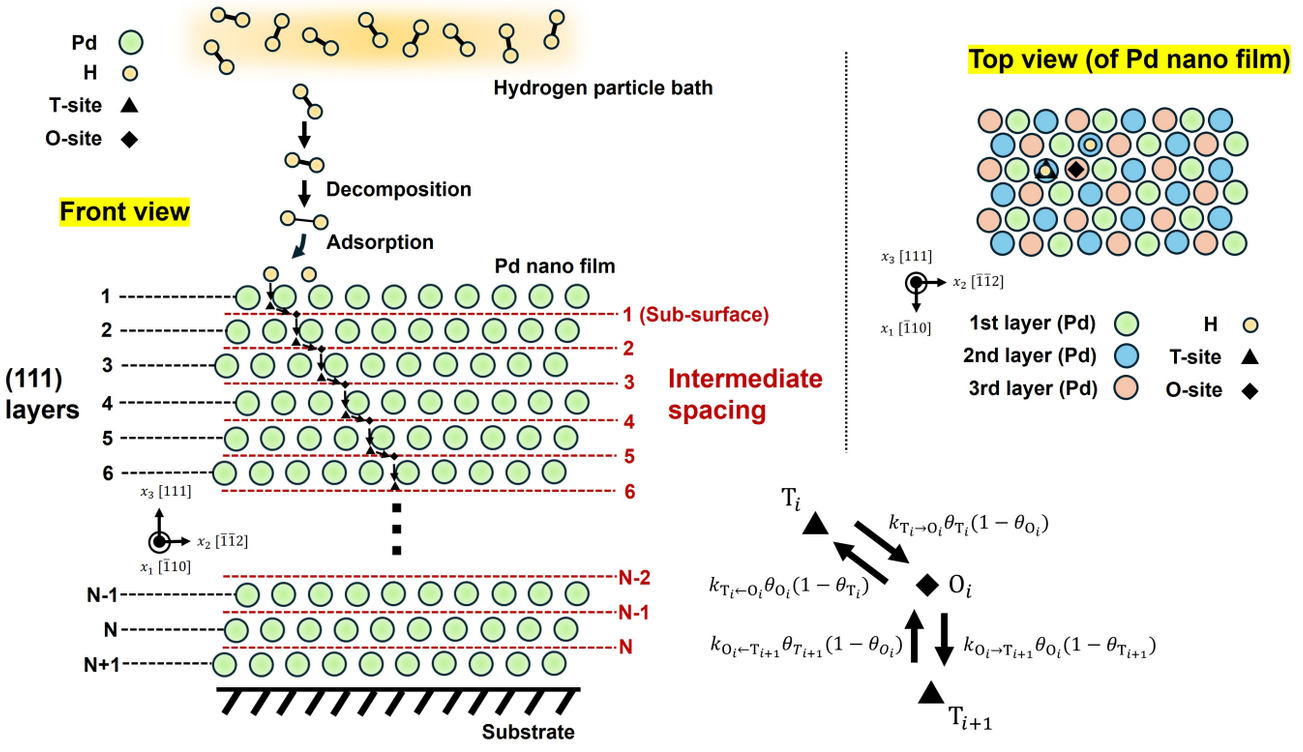

FIG. 1. Schematic of hydrogen adsorption and diffusion in Pd nano films with the (111) surface.

B. DFT atomistic simulation

Fig. 2 shows the schematic for calculating ΔE and ν using energetics from the DFT atomistic simulation. Once we calculate the potential energy change along the minimum energy path (MEP) between the two sites of the hydrogen atom in a potential energy surface, X and Y, $\Delta E_{\mathrm{X}\to\mathrm{Y}}$ ($\Delta E_{\mathrm{X}\leftarrow\mathrm{Y}}$) is calculated as the energy difference between the top of the potential energy curve (saddle point) and X (Y)[26]. Further, $\nu_{\mathrm{X}\to\mathrm{Y}}$ ($\nu_{\mathrm{X}\leftarrow\mathrm{Y}}$) is calculated by the curvature of the potential energy around X (Y). We fitted the potential energy change around X (Y) to a simple harmonic function $f(x_{\mathrm{H}}) = \frac{1}{2}a\eta_{\mathrm{H}}^2$ (a represents a fitting parameter and η_{H} represents the change in the position of the hydrogen atom along MEP). Then, ν is calculated as

$$\nu \equiv \sqrt{\frac{1}{m_{\mathrm{H}}}\frac{d^2 f}{d\eta_{\mathrm{H}}^2}} = \sqrt{\frac{a}{m_{\mathrm{H}}}}, \tag{4}$$

where m_{H} represents the mass of the hydrogen atom.

Fig. 3 shows atomic models used for the DFT calculation of potential energy along the MEP. A Pd nanofilm model with a (111) surface (216 atoms) was prepared, as shown in Fig. 3 (a), and a hydrogen atom was placed at the surface (red circle), each T or O site (triangle and diamond) in the Pd nano film up to the middle of the film (O_6) and atomic structure, including the cell shape, was optimized. Subsequently, the MEP of hydrogen diffusion between the two sites and the potential energy change along them were calculated using the drag method[27], constraining the movement of hydrogen along the diffusion path. We prepared atomic models, as shown in Fig. 3 (b), to calculate the energetics of hydrogen adsorption on the Pd (111) surface and the decomposition of hydrogen molecules into atoms. In Model (I), we placed one hydrogen molecule far from the Pd (111) surface of the atomic model (a); the distance between them was 4.0 Å and the atomic structure was optimized, which mimicks the state in which the hydrogen molecule is fully dissociated from the Pd (111) surface. We confirmed that the distance between the hydrogen molecule and Pd (111) surface did not change after structural optimization. We placed one hydrogen molecule close to the Pd (111) surface of the atomic model (a); the distance between them was 2.0 Å, and we obtained the atomic structure of Model (II) after structural optimization. The decomposition of hydrogen molecules and the adsorption to the Pd (111) surface occurred spontaneously during structural optimization. Then, the MEP and potential energy change

along it between Models (I) and (II) were investigated using the drag method, constraining the distance between the hydrogen molecule and the Pd (111) surface along the $\boldsymbol{x}_3$ direction.

DFT atomistic simulations were performed using the Vienna Ab initio Simulation Package[28]. The electron–ion interactions were described using the projector-augmented wave method[29]. The exchange correlation between electrons was treated using the Perdew–Burke–Ernzerhof generalized gradient approximation[30] with an energy cutoff of 520 eV for the plane-wave basis set. The energy convergence criteria for the electronic and ionic structure relaxations were set to 1.0×10^{-6} and 1.0×10^{-3} eV, respectively. A $3 \times 3 \times 1$ k-point mesh was used uniformly for all DFT simulations. The initial estimate for MEP were obtained through linear interpolation between each of the two sites, and 13 atomic models of the intermediate states were produced at equal intervals along the path for the drag method. Cell shapes of the atomic models were optimized during the MEP calculations using the drag method.

Fig. 4 shows the calculated potential energy change along MEP for (a) hydrogen adsorption on the Pd (111) surface and decomposition of the hydrogen molecule and (b) hydrogen diffusion into the Pd nano film. Fig. 4 (b) show that the potential energy change of the hydrogen atom diffusion *only* up to O_3-site because the calculated potential energy change beneath the site is the iteration of that between O_2 to O_3, which suggests the effect of the Pd (111) surface to the hydrogen diffusion is only up to the subsurface. The calculated values of ΔE and ν for each hydrogen transition event are summarized in Table I. The overall values of ν in the table do not differ significantly from the conventionally used value $\nu = 1.0 \times 10^{13}$ 1/s; the order of the frequencies is almost the same, and the effect of the change in ν caused by the potential energy landscape on the hydrogen concentration may not be significant.

From DFT simulations, we confirmed that hydrogen decomposition and adsorption to the (111) surface of the Pd nano films occurred simultaneously, and the distance between the hydrogen molecule and surface was 2.4 Å at the saddle point, as shown in Fig. 4 (a). The difference in the activation energy between the forward (adsorption) and backward (dissociation) process is considerably large; $\Delta E_{(\mathrm{H_2} \rightarrow \mathrm{S})} = 0.10$ and $\Delta E_{(\mathrm{H_2} \leftarrow \mathrm{S})} = 1.08$ eV as in Table I, which suggests the rapid adsorption of hydrogen on the surface. For the diffusion of hydrogen atoms into the Pd nano films, as shown in Fig. 4 (b) and Table I, the difference in the activation energies between forward and backward diffusion processes is large between the surface and T_1 site in the subsurface. $\Delta E_{(\mathrm{S} \rightarrow \mathrm{T_1})} = 0.36$ and $\Delta E_{(\mathrm{S} \leftarrow \mathrm{T_1})} = 0.01$ eV,

which suggests that hydrogen atoms tend to accumulate on the surface and the invasion of hydrogen into the Pd bulk is difficult. The potential energy change between O_1 to T_2, $\Delta E_{(O_1 \rightarrow T_2)} = 0.33$, and $\Delta E_{(O_1 \leftarrow T_2)} = 0.16$ eV indicates that there is a relatively small energetic obstacle for the diffusion from the O site in the subsurface to the T site of the next (111) layer, suggesting that the accumulation of hydrogen in subsurface is possible. The potential energy change beneath O_2 sites is the iteration between O_2 and O_3. The concentration at the site beneath O_2 sites does not depend on the depth of the layer at the equilibrium state.

Fig. 4 (b) and Table I show that the value of activation energy between in- and out-plane diffusion is different, e.g., $\Delta E_{(T_3 \rightarrow O_3)} = 0.10$ (in-plane) and $\Delta E_{(O_2 \leftarrow T_3)} = 0.14$ eV (out-plane). The activation energy of the out-plane diffusion is always 0.04 eV higher than that of the in-plane diffusion. We confirmed that this difference is caused by the atomic models we used. The size of the atomic model is limited because of the cost of DFT calculations, and the area of the (111) plane is only 120 $Å^2$. The corresponding hydrogen concentration between planes becomes 6 %atom if a hydrogen atom is placed at a certain sites between certain (111) planes because of the periodicity of the models. This highly concentrated hydrogen atoms enlarge the width between (111) planes and increase the activation energy of out-plane diffusion. Further, we confirmed the activation energy of T $\rightarrow$ O (T $\leftarrow$ O) diffusion in FCC Pd bulk atomic model is 0.10 and 0.16 eV, which is the same as the those of in-plane diffusion.

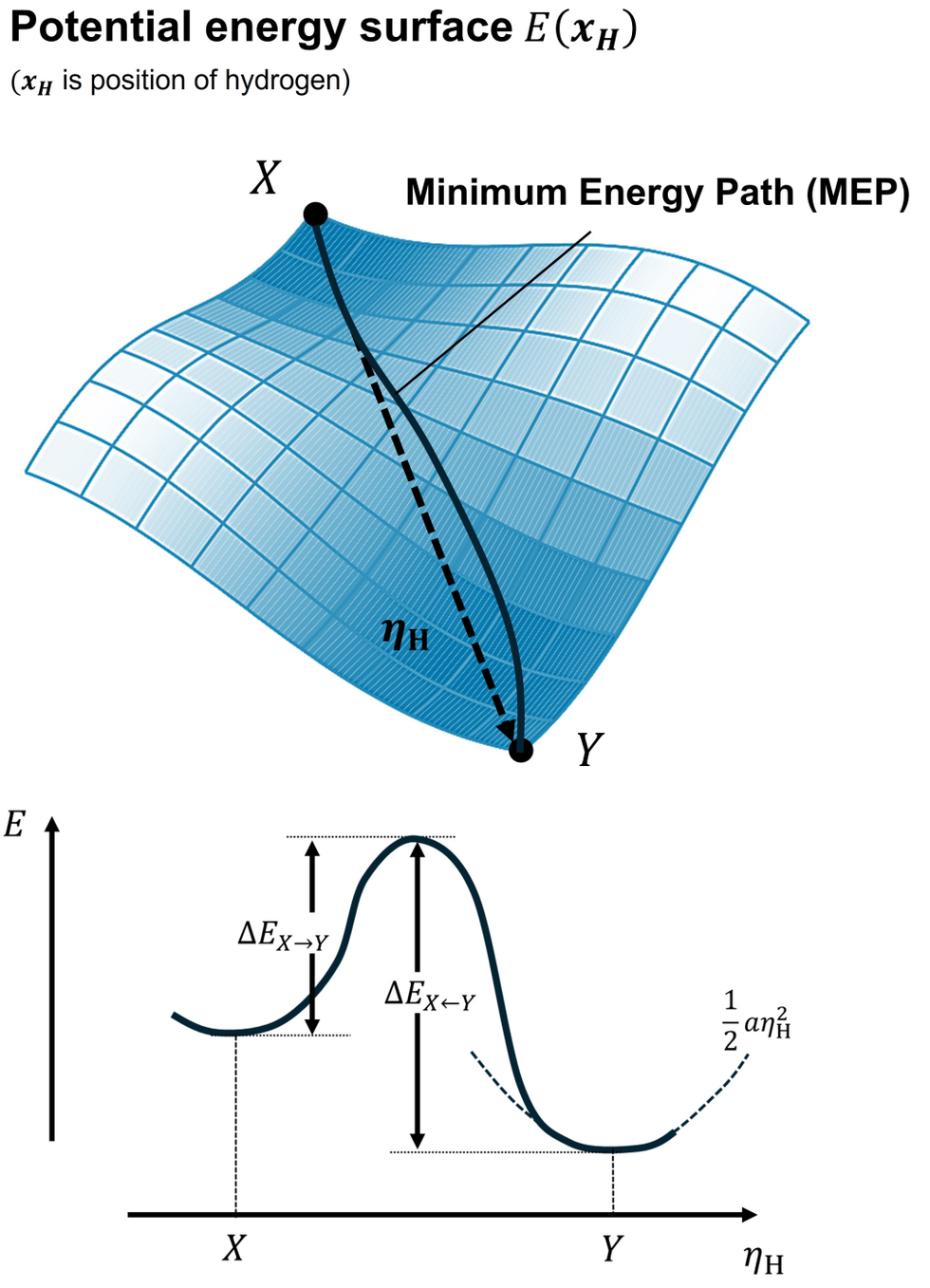

FIG. 2. Schematic for calculating ΔE and ν; potential energy surface and potential energy change along the minimum energy path (MEP).

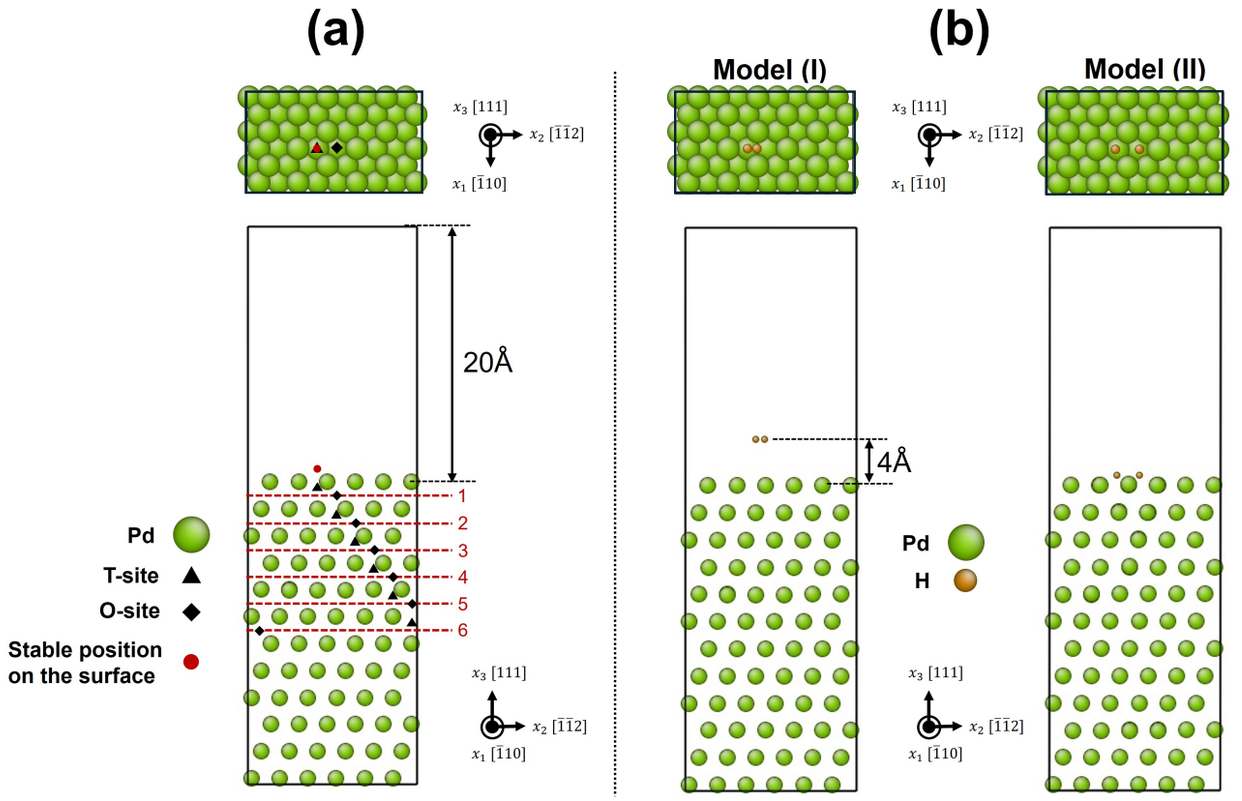

FIG. 3. Atomic models used for DFT atomistic simulation. (a) Pd nano film model with (111) surface (216 atoms); the black lines indicate the supercell. Hydrogen atoms were put at a stable position on the (111) surface (red circle), T site (black triangles), and O site (black diamonds) positions to investigate the energetics of hydrogen diffusion from (111) surface to the inside of the Pd nano film. (b) Atomic models to investigate the energetics of hydrogen adsorption on the Pd (111) surface and decomposition of the hydrogen molecule to atoms. The atomic structures are visualized using the AtomEye software[31].

TABLE I. Calculated values of the activation energies and jump frequencies of hydrogen adsorption and diffusion in the Pd nano film.

	Forward ($\bigstar = \rightarrow$)	Backward ($\bigstar = \leftarrow$)
$\Delta E_{(\mathrm{H_2} \bigstar \mathrm{S})}$	0.10 eV	1.08 eV
$\Delta E_{(\mathrm{S} \bigstar \mathrm{T_1})}$	0.36 eV	0.01 eV
$\Delta E_{(\mathrm{T_1} \bigstar \mathrm{O_1})}$	0.12 eV	0.12 eV
$\Delta E_{(\mathrm{O_1} \bigstar \mathrm{T_2})}$	0.33 eV	0.16 eV
$\Delta E_{(\mathrm{T_2} \bigstar \mathrm{O_2})}$	0.10 eV	0.13 eV
$\Delta E_{(\mathrm{O_2} \bigstar \mathrm{T_3})}$	0.20 eV	0.14 eV
$\Delta E_{(\mathrm{T_3} \bigstar \mathrm{O_3})}$	0.10 eV	0.16 eV
$\nu_{(\mathrm{H_2} \bigstar \mathrm{S})}$	–	9.56×10^{12} 1/s
$\nu_{(\mathrm{S} \bigstar \mathrm{T_1})}$	1.21×10^{13} 1/s	3.91×10^{12} 1/s
$\nu_{(\mathrm{T_1} \bigstar \mathrm{O_1})}$	1.03×10^{13} 1/s	7.89×10^{12} 1/s
$\nu_{(\mathrm{O_1} \bigstar \mathrm{T_2})}$	6.91×10^{12} 1/s	1.08×10^{13} 1/s
$\nu_{(\mathrm{T_2} \bigstar \mathrm{O_2})}$	9.59×10^{13} 1/s	5.87×10^{12} 1/s
$\nu_{(\mathrm{O_2} \bigstar \mathrm{T_3})}$	7.57×10^{12} 1/s	1.16×10^{13} 1/s
$\nu_{(\mathrm{T_3} \bigstar \mathrm{O_3})}$	1.01×10^{13} 1/s	6.49×10^{12} 1/s

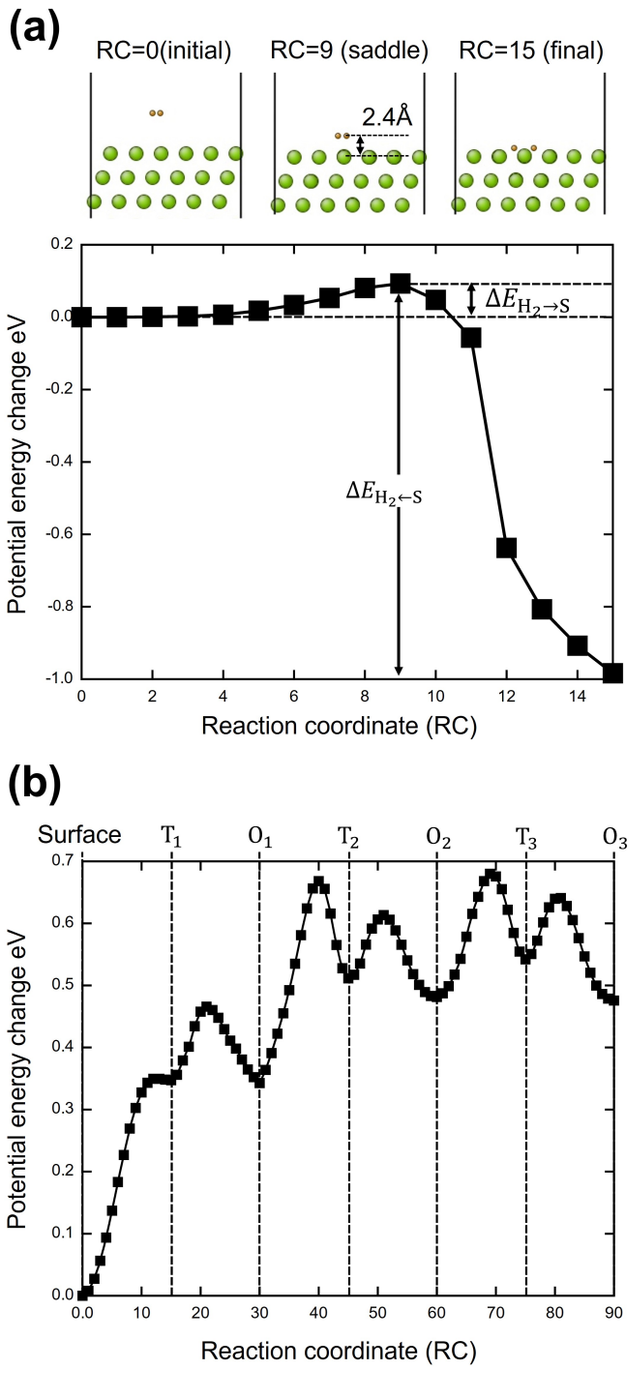

FIG. 4. DFT calculated energetics of hydrogen adsorption and diffusion in Pd nano films. (a) The potential energy change for the decomposition of hydrogen molecule and adsorption of the hydrogen atom to the Pd (111) surface. (b) The potential energy change for the diffusion of hydrogen atom into the Pd nano film. The standard of the potential energy is set as the potential energy of the initial state of each plot and the curves in the plots are guides of the eyes.

III. RESULT AND DISCUSSION

Using the calculated values in Table I and equations (1), (2), and (3), we numerically calculated the temporal evolution of the θ of the surface (coverage) and each sites in Pd nano films in a large time scale from 1.0×10^{-15} to 2.0×10^{2} s, setting the condition as $T = 300$ K and $p_{\mathrm{H_2}} = 10$, 100, 1000, and 10000 ppm (1.0 atm). The time step Δt for the numerical calculation is set as 1.0×10^{-15} s and the initial values of all θ were set to zero. Note that $N = 20$ is used and $n_s = 1.51 \times 10^{19}$ 1/m^2 is calculated from the size of our atomic models. We confirmed the value of N does not affect the result very much; we got almost same result with $N = 7$.

The calculated results are shown in Fig. 5. The temporal evolution of coverage θ_{S}, concentrations in subsurfaces $\theta_{\mathrm{T_1}}$ and $\theta_{\mathrm{O_1}}$, and concentrations in the 5th intermediate spacing (from the surface) $\theta_{\mathrm{T_5}}$ and $\theta_{\mathrm{O_5}}$ are shown. We confirmed that the concentrations of each site in the intermediate spacing beneath the subsurface were almost uniform, and therefore, only concentrations in the 5th intermediate spacing are shown in the plot, which represents the concentrations in the bulk. As a result, the coverage θ_{S} reached 1.0 in a considerably short time for all ppm conditions: to the order of 10^{-5} to 10^{-2} s, which suggests that the Pd surface is always fully covered in the time scale of conventional experiments, 10^{0} to 10^{2} s, under exposure to hydrogen gas[14,15]. The concentrations of the sites in the subsurface depends on the hydrogen gas pressure and only reached 0.07, 0.14, 0.28, and 0.55 after the surface is fully covered by hydrogen atoms at 10, 100, 1000, and 10000 ppm, respectively, under 200 s of exposure to hydrogen gas. The hydrogen concentration in the bulk exhibited the same trend; however, the change is relatively small for all cases: to the order of 10^{-5} to 10^{-3}. As shown in Table I, this is caused by the low activation energy of hydrogen adsorption and backward diffusion from the subsurface to the surface. The concentrations of the T sites were generally considerably smaller than those of the O sites in the bulk, which reflects the energy landscape of hydrogen diffusion in Fig. 4 (b). O sites are more stable than T sites in Pd for hydrogen beneath the sub-surface. In contrast, concentrations of both T and O sites are similar in the subsurface, which reflects the fact that the energy difference between them in the subsurface ($\mathrm{T_1}$ and $\mathrm{O_1}$) is considerably smaller than that in the bulk.

We selected $\theta_{\mathrm{O_5}}$ and re-plot it in Fig. 6 (a) to compare our results with the experimental observations. The change in $\theta_{\mathrm{O_5}}$ at 200 s with respect to hydrogen gas pressure (ppm) is

also plotted in Fig. 6 (b). Fig. 6 (b) shows that the concentration of hydrogen increases rapidly at 10000 ppm and reaches 0.4 % from the 0.01 % order at 10 ppm. This trend is similar to the experimentally observed increase in resistance. Wagner et al. investigated the electric resistance change of Pd nano films with respect to the pressure of hydrogen gas and observed similar rapid changes around 10000 ppm (1.0 atm) for the nano films bonding on the substrate[17]. Therefore, our analysis suggests that a 0.1% change in the hydrogen concentration in the bulk significantly affects the resistance. Fig. 6 (a) shows that the 10^1 to 10^2 s order time are necessary for increasing the 0.1% order concentration for 10000 ppm. This is consistent with the temporal resistance change of Pd nanofilms observed experimentally by Lee et al. The time scale of the resistance change is actually in 10^1 to 10^2 s order[14]. In our calculations, the concentration reached 90 % of that at 200 s after approximately 130 s. Actually, Lee et al. reported a response time of 130 s, which was the time required to reach 90 % of the total change in the electrical resistance of the Pd nano film. The shape of the concentration curve shown in Fig. 6 (a) is considerably similar to the experimentally observed curves of the resistance change[14,15] or the hydrogen profile changes[10,11] with respect to time, thereby confirming that the kinetic model itself does reproduce the kinetics of the hydrogen solution in Pd nano films though it is simple.

We also calculated the time-dependent diffusion coefficient of the hydrogen intrusion $D_{x_3}(t)$ in the Pd bulk by finite-difference method using the calculated temporal evolution of the concentration and Fick's second law,

$$\frac{\partial \theta}{\partial t} = D_{x_3} \frac{\partial^2 \theta}{\partial x_3^2}.$$

$D_{x_3}(t)$ was calculated at O_5 and the spacial difference of the concentration along $\boldsymbol{x_3}$ $\left(\frac{\partial^2 \theta}{\partial x_3^2}\right)$ was calculated using the hydrogen concentration at O_5, O_4 and O_6, and the width of intermediate spacing between the adjacent layers $\Delta x_3 = 0.23$ nm. We show the result in Fig. 7. Generally, as time increases (the concentration reaches to the equilibrium), the diffusion coefficient decreases approximately in proportion to $1/t$. Time-dependent decay of the diffusion coefficient was discussed using fluctuation-dissipation theorem from old times[32] and similar type of the decay to our result was theoretically discussed for the polarons in organic semicondactors in the literature[33]. In our case, the temporal dependency of D_{x_3} originates from the description of the flux in our kinetic model; our flux is not simple form as Fick's

first law $J = -D_{x_3}\frac{\partial\theta}{\partial x_3}$ (J is flux), in which the flux is the function of only the spacial gradient of the concentration. The partial pressure of the hydrogen gas does not affect D_{x_3} very much and this is because the diffusion in Pd bulk always occurs after the surface is fully covered by the hydrogen atoms from Fig. 5. The driving force for hydrogen intrusion in Pd bulk is due to the highly hydrogen concentrated surface rather than the hydrogen gas itself. Li et al. experimentally observed the diffusion coefficient of hydrogen in Pd nano film by the electrochemical stripping method[34] as 2.1×10^{-11} cm^2/s , which is consistent with our diffusion coefficient in early time (from 0.01 to 0.1 s) in Fig. 7. This relatively large diffusion coefficient in experiment may be due to the constant driving force of the electric potential and the existence of another intrusion or diffusion paths like grain boundaries.

We also implemented the same analysis by changing the temperature to 400 and 200 K to investigate the effect of temperature on the concentration; the results are presented in Figs. 8 and 9. Fig. 8 indicates that the system reached thermal equilibrium because all θ becomes constant with respect to the time at certain time at 400 K. Values of the equilibrium hydrogen concentrations in the subsurface and bulk were not 1.0, and they depended on the value of the hydrogen gas pressure p_{H_2}. In contrast, all concentrations at 200 K, except for coverage, were considerably lower than those at 300 K (Fig. 9).

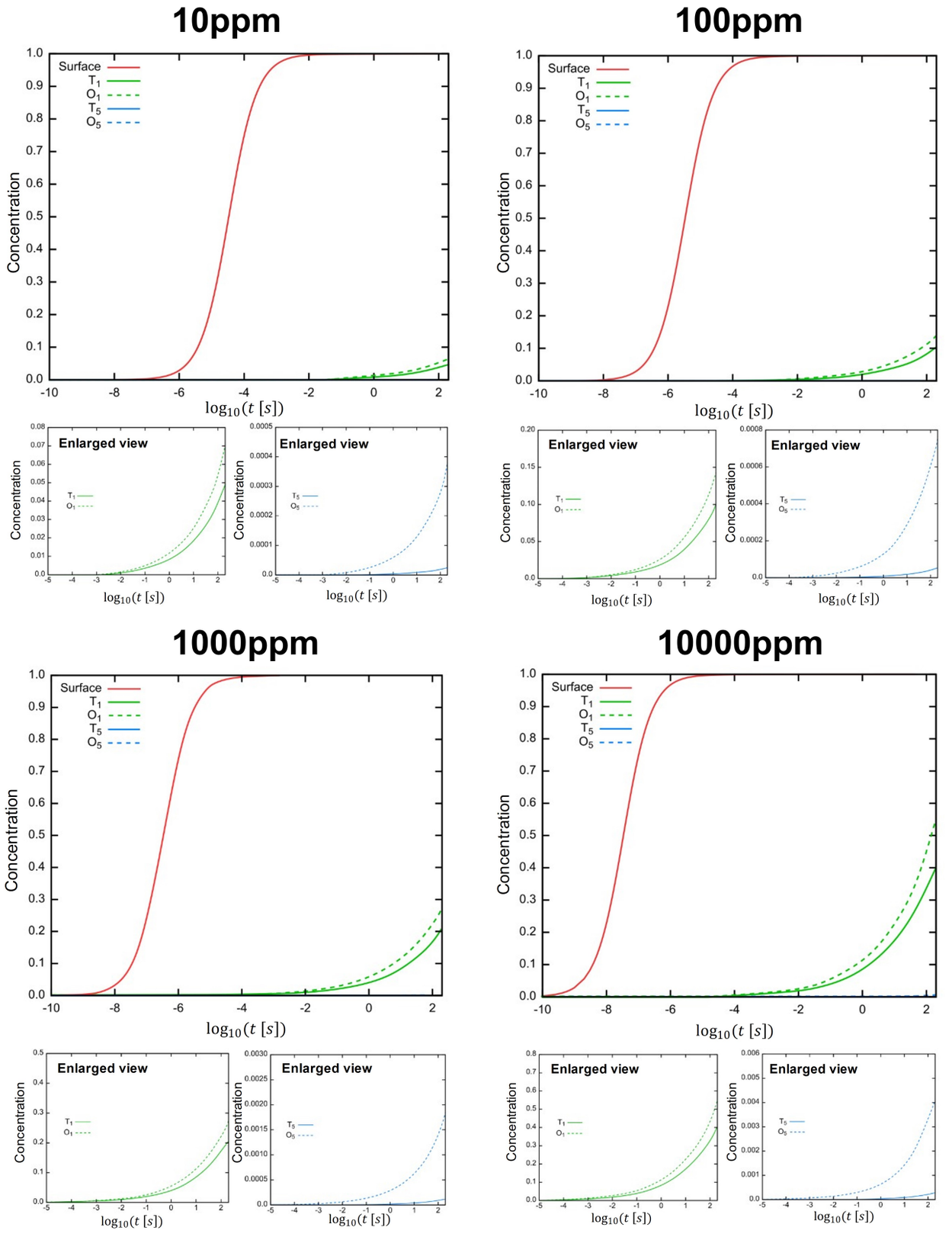

FIG. 5. Temporal evolution of θ_S, θ_{T_1}, θ_{O_1}, θ_{T_5}, and θ_{O_5} at 300 K.

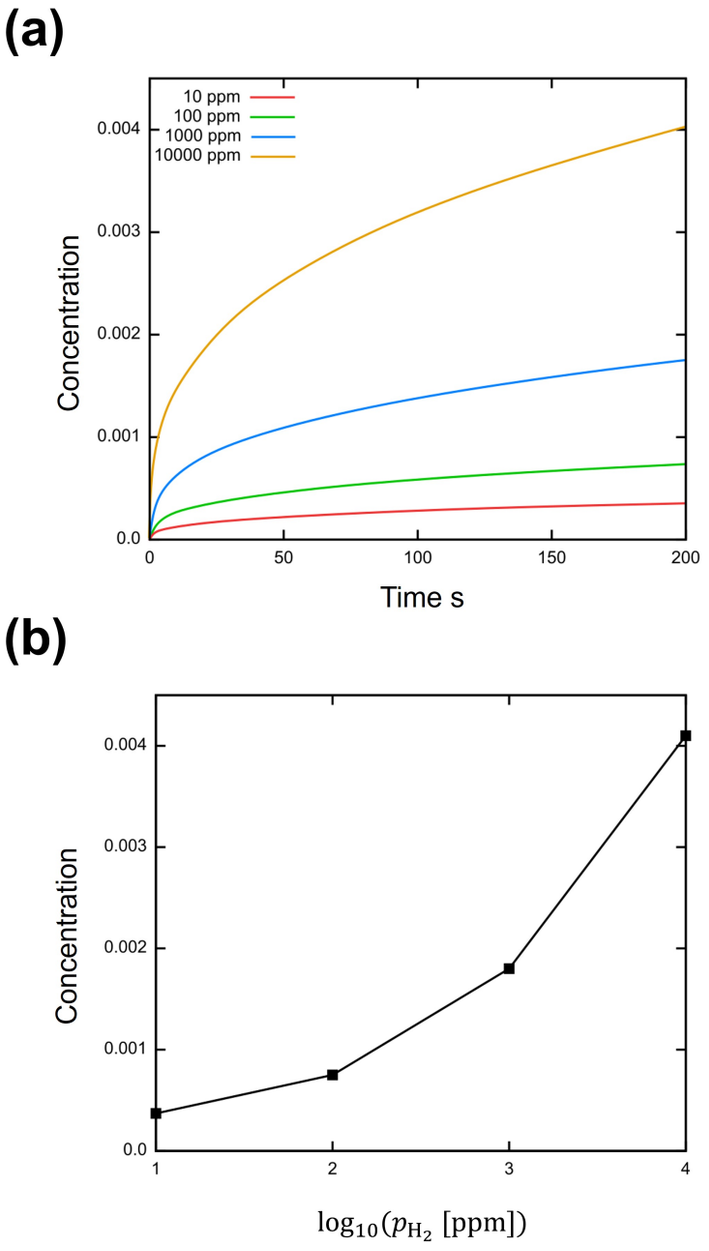

FIG. 6. Hydrogen gas pressure and temporal dependencies of θ_{O_5} at 300 K. (a) Temporal evolution of θ_{O_5} for each hydrogen gas pressure. (b) Hydrogen gas pressure vs. θ_{O_5} at a 200 s plot.

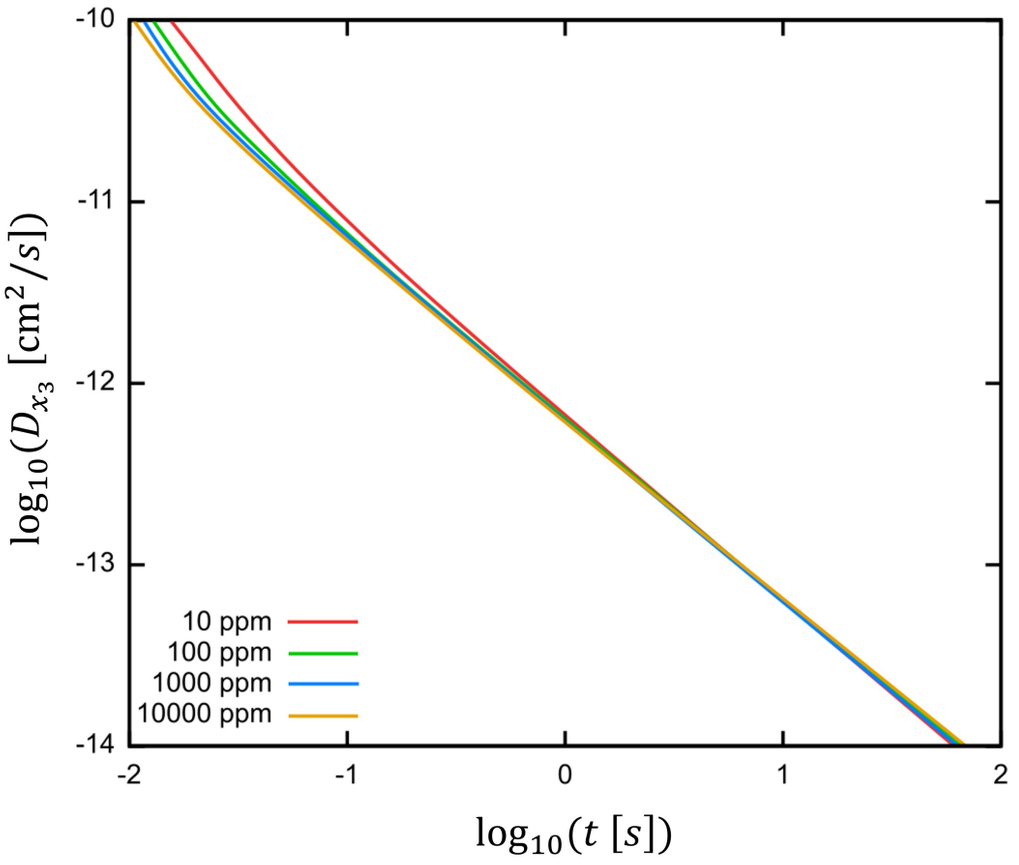

FIG. 7. Temporal dependency of the diffusion coefficient of hydrogen in Pd bulk (at O_5 site).

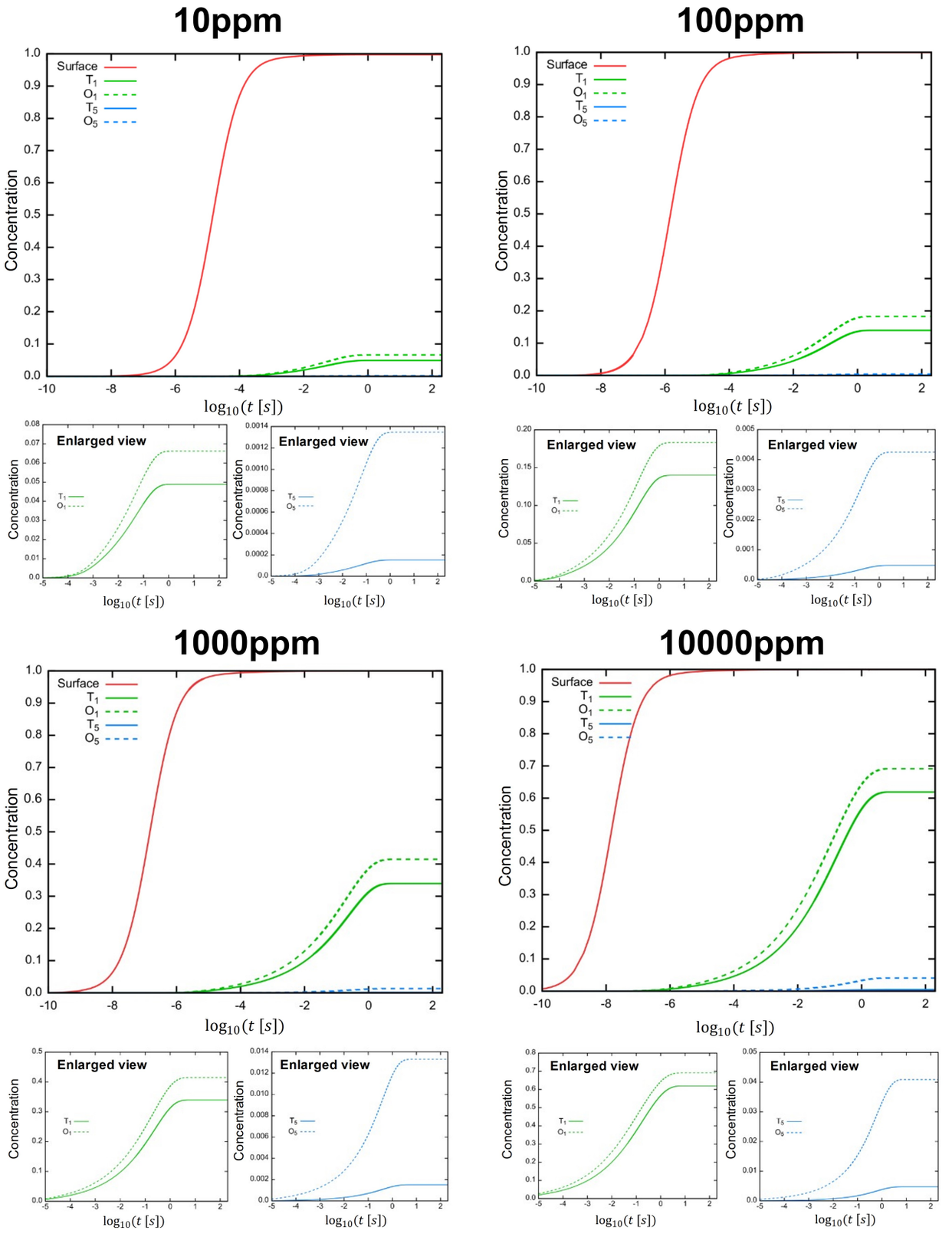

FIG. 8. Temporal evolution of θ_{S}, θ_{T_1}, θ_{O_1}, θ_{T_5}, and θ_{O_5} at 400 K.

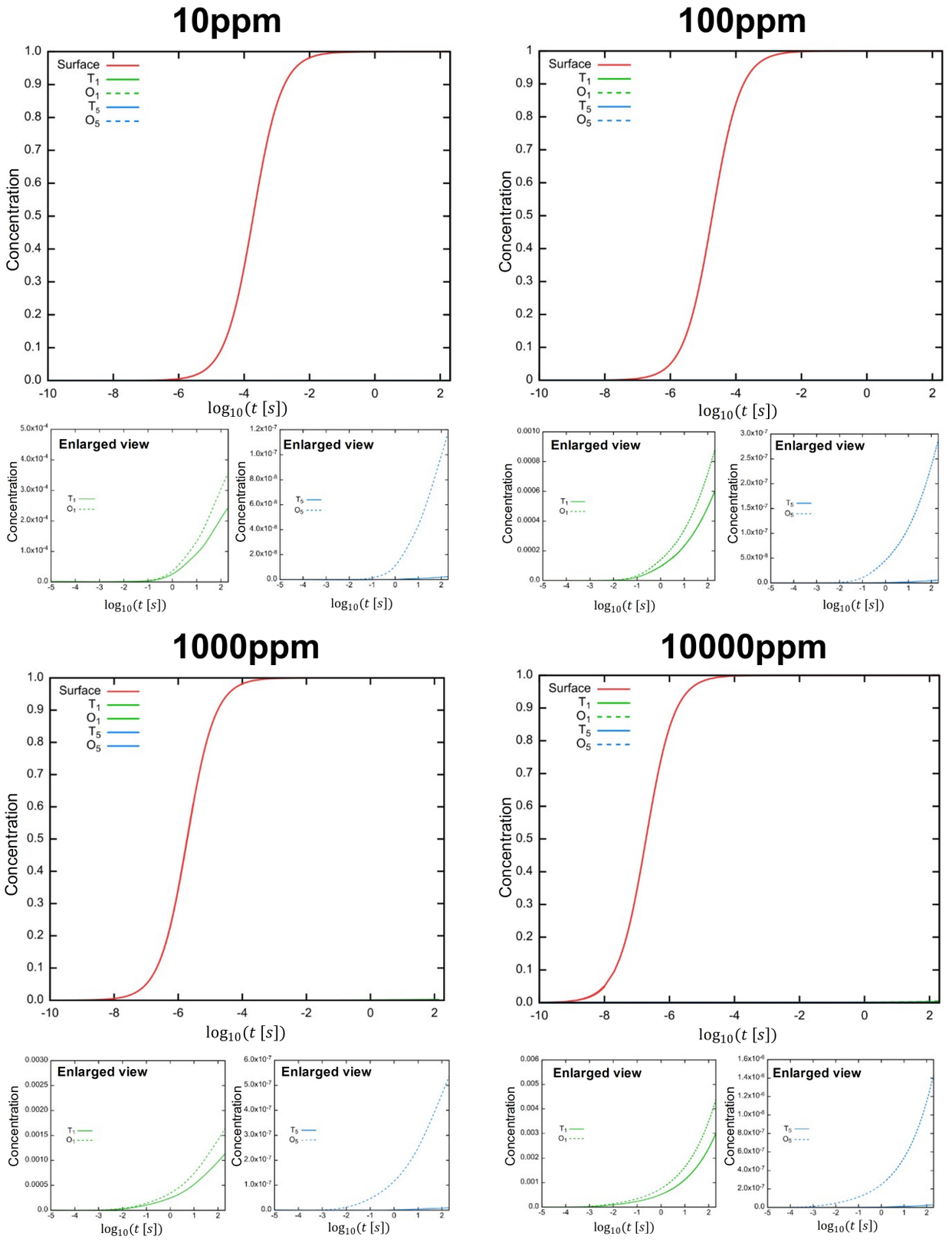

FIG. 9. Temporal evolution of θ_{S}, θ_{T_1}, θ_{O_1}, θ_{T_5}, and θ_{O_5} at 200 K.

IV. SUMMARY

We proposed a parameter-free multiscale analysis of hydrogen solubility in FCC Pd nano films with the (111) surface under hydrogen gas conditions using DFT atomisitic simulations and a simple kinetic model. The calculated solubility was quantitatively analyzed and compared with the experimental observations. Although the Pd surface is fully covered by hydrogen atoms in a short time, the hydrogen concentration in the subsurface or bulk changes significantly on the experimental time scale due to the exposure to 10 to 10000 ppm hydrogen gas (1.0 atm) depending on the gas pressure. Through comparison between the calculated hydrogen concentration and experimental observations of electric resistance change attributed to the exposure of hydrogen gas, we concluded that the hydrogen concentration in the bulk or subsurface of Pd nano films plays a role in changing the resistance of Pd. A 0.1 % change in the hydrogen concentration in the bulk may be necessary to observe a significant change in the electric resistance as a hydrogen sensor. Further, we calculated the time-dependent diffusion coefficient of hydrogen in Pd nano film and compared it with experimental observed one. We also investigated temperature dependency of the solubility and we confirmed that the hydrogen gas pressure determines hydrogen solubility in the Pd nano films at the equilibrium state, whereas the temperature controls the speed to reach the equilibrium state. Finally, we need to mention that our multiscale analysis approach is generally useful for the quantitative analysis of the kinetics of interstitial diffusion in solid materials through the surface. We plan to apply our method to quantitatively investigate the hydrogen concentration in such materials because it is well known that hydrogen has a negative effect on the mechanical properties of conventional structural materials[35–37].

APPENDIX

AUTHOR DECLARATIONS

Conflict of Interest

The authors declare no conflict of interest.

Author Contributions

Akio Ishii Conceptualization (lead); Formal analysis (equal); Investigation (equal); Software (lead); Writing - Original draft preparation (lead); Writing - Review & editing (equal)

Nobutomo Nakamura Investigation (equal); Formal analysis (equal); Writing - Original draft preparation (supporting); Writing - Review & editing (equal)

DATA AVAILABILITY

The data supporting the findings of this study are available from the corresponding author upon reasonable request.

ACKNOWLEDGMENT

This study was partially supported by a Grant-in-Aid for Scientific Research 23K20037 from the Japan Society for the Promotion of Science. The DFT simulations were partly performed using SQUID large-scale computer systems at the Cybermedia Center, Osaka University.

REFERENCES

[1]C. M. Welch and R. G. Compton, "The use of nanoparticles in electroanalysis: a review," Anal. Bioanal. Chem. **384**, 601–619 (2006).

[2]V. Mohanraj and Chen, "Nanoparticles-a review," Trop. J. pharm. res. **5**, 561–573 (2006).

[3]R. Ferrando, J. Jellinek, and R. L. Johnston, "Nanoalloys: From theory to applications of alloy clusters and nanoparticles," Chem. Revi. **108**, 845–910 (2008).

[4]N. Nakamura, K. Matsuura, A. Ishii, and H. Ogi, "Restructuring in bimetallic core-shell nanoparticles: Real-time observation," Phys. Rev. B **105**, 125401 (2022).

[5]N. Nakamura, K. Matsuura, and A. Ishii, "In situ observation of morphological change of Pd-based bimetallic nanoparticles synthesized by co-sputtering," J. Appl. Phys. **134**, 145301 (2023).

[6]A. Ishii, "Energetical effects of the edges and vertices of face-centered-cubic Pd and Au nanoparticles: A density functional theory study," Comput. Mater. Sci. **243**, 113122 (2024).

[7]V. Kafil, B. Sreenan, M. Hadj-Nacer, Y. Wang, J. Yoon, M. Greiner, P. Chu, X. Wang, M. S. Fadali, and X. Zhu, "Review of noble metal and metal-oxide-semiconductor based chemiresistive hydrogen sensors," Sens. Actuators A Phys. **373**, 115440 (2024).

[8]A. Ishii, "Edge- and vertex-originated differences between nanoparticles and nanovoids: A density functional theory study of face-centered-cubic Al," Comput. Mater. Sci. **246**, 113342 (2025).

[9]A. Viola, R. Chattot, V. Martin, G. Tsirlina, J. Nelayah, J. Drnec, and F. Maillard, "Hydrogen Trapping in Palladium Nanoparticles Revealed by Electrochemical, X-ray Scattering, and Spectrometric Measurements," J. Phys. Chem. C **127**, 17761–17769 (2023).

[10]G. Li, H. Kobayashi, J. M. Taylor, R. Ikeda, Y. Kubota, K. Kato, M. Takata, T. Yamamoto, S. Toh, S. Matsumura, and H. Kitagawa, "Hydrogen storage in Pd nanocrystals covered with a metal-organic framework," Nature Mater. **13**, 802–806 (2014).

[11]G. Li, H. Kobayashi, S. Dekura, R. Ikeda, Y. Kubota, K. Kato, M. Takata, T. Yamamoto, S. Matsumura, and H. Kitagawa, "Shape-Dependent Hydrogen-Storage Properties in Pd Nanocrystals: Which Does Hydrogen Prefer, Octahedron (111) or Cube (100)?" J. Amer. Chem. Soc. **136**, 10222–10225 (2014).

[12]Z. Chen, X. Wu, H. Liu, M. A. Baqir, K. Yu, and K. Zhang, "Hyperbolic metamaterials assisted ultrathin Pd films for high-sensitivity hydrogen sensors," Inter. J. Hydr. Ene. **81**, 812–818 (2024).

[13]A. Ishii and N. Nakamura, "Ab initio morphology prediction of Pd, Ag, Au, and Pt nanoparticles on (0001) sapphire substrates," J. Appl. Phys. **135**, 094301 (2024).

[14]E. Lee, J. M. Lee, J. H. Koo, W. Lee, and T. Lee, "Hysteresis behavior of electrical resistance in Pd thin films during the process of absorption and desorption of hydrogen gas," Inter. J. Hydr. Ene. **35**, 6984–6991 (2010).

[15]N. Nakamura, T. Ueno, and H. Ogi, "Hydrogen-gas sensing at low concentrations using extremely narrow gap palladium nanoclusters prepared by resistive spectroscopy," J. Appl. Phys. **126**, 225104 (2019).

[16]N. Nakamura, K. Yoshikawa, and A. Ishii, "Enhancement of hydrogen response by forming an Au submonolayer on nanogap Pd nanoparticles," Appl. Phys. Lett. **125**, 021902 (2024).

[17]S. Wagner and A. Pundt, "Electrical resistivity and hydrogen solubility of PdHc thin films," Acta Mater. **58**, 1387–1394 (2010).

[18]R. J. Behm, V. Penka, M. G. Cattania, K. Christmann, and G. Ertl, "Evidence for "subsurface" hydrogen on Pd(110): An intermediate between chemisorbed and dissolved species," J. Chem. Phys. **78**, 7486–7490 (1982).

[19]H. Okuyama, T. Nakagawa, W. Siga, N. Takagi, M. Nishijima, and T. Aruga, "Subsurface hydrogen at Pd(100) induced by gas-phase atomic hydrogen," J. Phys. Chem. B **103**, 7876–7881 (1999).

[20]K. Namba, S. Ogura, S. Ohno, W. Di, K. Kato, M. Wilde, I. Pletikosic, P. Pervan, M. Milun, and K. Fukutani, "Acceleration of hydrogen absorption by palladium through surface alloying with gold," Proc. Natl. Acad. Sci. U. S. A., **115**, 7896–7900 (2018).

[21]M. Blanco-Rey and J. C. Tremblay, "Diffusion of hydrogen interstitials in the near-surface region of Pd(111) under the influence of surface coverage and external static electric fields," J. Chem. Phys. **142**, 154704 (2015).

[22]J. W. Davenport, G. J. Dienes, and R. A. Johnson, "Surface effects on the kinetics of hydrogen absorption by metals," Phys. Rev. B **25**, 2165–2174 (1982).

[23]J. E. Mueller, P. Krtil, L. A. Kibler, and T. Jacob, Phys. Chem. Chem. Phys. **16**, 15029–15042 (2014).

[24]L. B. Loeb, *The kinetic theory of gases* (Dover Publications, 1961).

[25]T. B. Delchar, *Vacuum Physics and Techniques* (Chapman and Hall, 1993).

[26]H. Miyoshi, H. Kimizuka, A. Ishii, and S. Ogata, "Temperature-dependent nucleation kinetics of Guinier-Preston zones in Al–Cu alloys: An atomistic kinetic Monte Carlo and classical nucleation theory approach," Acta Mater. **179**, 262–272 (2019).

[27]H. Jonsson, G. Mills, and K. W. Jacobsen, "Nudged elastic band method for finding minimum energy paths of transitions, in: B.j. berne, g. ciccotti, d.f. coker (eds.), classical," in *Classical and Quantum Dynamics In Condensed Phase Simulations* (World Scientific, Singapore, 1998).

[28]G. Kresse and J. Furthmüller, Physi. Rev. B **54**, 11169–11186 (1996).

[29]G. Kresse and D. Joubert, Phys. Rev. B **59**, 11–19 (1999).

[30]J. Perdew, K. Burke, and M. Ernzerhof, Phys. Rev. Lett. **77**, 3865–3868 (1996).

[31]J. Li, "AtomEye: An efficient atomistic configuration viewer," Model. Sim. Mater. Sci. Eng. **11**, 173–177 (2003).

[32]X. Bian, C. Kim, and G. E. Karniadakis, "111 years of Brownian motion," Soft Matter **12**, 6331–6346 (2016).

[33]D. Rais, M. Menšík, B. Paruzel, P. Toman, and J. Pfleger, "Concept of the Time-Dependent Diffusion Coefficient of Polarons in Organic Semiconductors and Its Determination from Time-Resolved Spectroscopy," J. Phys. Chem. C **122**, 22876–22883 (2018).

[34]Y. Li and Y. T. Cheng, "Hydrogen diffusion and solubility in palladium thin films," Inter. J. Hydr. Ene. **21**, 281–291 (1996).

[35]M. C. Tiegel, M. L. Martin, A. K. Lehmberg, M. Deutges, C. Borchers, and R. Kirchheim, "Crack and blister initiation and growth in purified iron due to hydrogen loading," Acta Mater. **115**, 24–34 (2016).

[36]L. Wan, W. T. Geng, A. Ishii, J.-P. Du, Q. Mei, N. Ishikawa, H. Kimizuka, and S. Ogata, "Hydrogen embrittlement controlled by reaction of dislocation with grain boundary in alpha-iron," Inter. J. Plast. **112**, 206–219 (2019).

[37]K. Horikawa and A. Ishii, "Effect of purity on the internal morphology of blisters on aluminum surfaces," Res. Mater. **21**, 100522 (2024).